

Schwarzschild Black Hole Turbulence: Scalar Probe

Alex Kehagias^a Antonio Riotto^b

^aPhysics Division, National Technical University of Athens, Athens, 15780, Greece

^bDepartment of Theoretical Physics and Gravitational Wave Science Center,
24 quai E. Ansermet, CH-1211 Geneva 4, Switzerland

E-mail: kehagias@mail.ntua.gr, antonio.riotto@unige.ch

Abstract. We explore how perturbations of a Schwarzschild black hole can redistribute energy among scalar modes and seed turbulent-like cascades. We make use of the van der Pol–Krylov–Bogoliubov averaging method and derive coupled mode equations that describe near-resonant interactions between neighboring multipoles. We compare two routes to instability, namely the difference-frequency mixing between adjacent modes and the diagonal (Mathieu) self-modulation channel. We show that, at high multipole number (eikonal limit), the difference-frequency route dominates and drives a one-way cascade from higher to lower frequencies. We chart the corresponding instability regions (“tongues”) and quantify their detuning dependence. The framework provides a simple, quantitative mechanism for energy transfer in black hole ringdowns and clarifies when and how turbulent signatures can arise within linear probes on a weakly perturbed background.

Contents

1	Introduction	1
2	Massless scalar on Perturbed Schwarzschild	2
3	Two-mode reduction	4
3.1	Off-diagonal, three-wave mixing channel	5
3.2	Diagonal Mathieu channel	7
4	Higher-order instability	9
5	Conclusions	11

1 Introduction

Quasi-Normal Modes (QNMs) constitute a defining feature of Black Holes (BHs), capturing their characteristic response to external disturbances (for a recent review, see Ref. [1]). By analyzing this response, one can extract valuable insights into the final stage of the merger between compact objects—the so-called ringdown—which marks the birth of a new BH. Accurately describing the ringdown phase is a fundamental aspect of the ongoing effort to interpret gravitational-wave observations from compact binary coalescences [2–8], as well as to prepare for analyses involving next-generation ground- and space-based detectors [9–12]. Although the current framework has yielded considerable success with existing data, several recent works [13–19] have emphasized that nonlinear gravitational effects can alter the expected QNM spectrum. In particular, these effects can introduce additional spectral peaks located at frequencies corresponding to linear frequency sums, often with appreciable amplitudes. A range of analytical and numerical investigations has been devoted to exploring these nonlinear oscillations [17–38]. These studies mainly focus on the quadratic quasi-normal mode 2ℓ arising from the coupling of two ℓ -multipoles, which could potentially be observable with future third-generation detectors for $\ell = 2$ [39–42].

However, how about the opposite process in which two large ℓ -modes annihilate to create a smaller ℓ -mode? Being of the interaction being of the same (cubic) order, one would expect that this process is equally taking place. This would be an inverse energy cascade, eventually terminating into the most observable mode $\ell = 2$. In fact, recently it has been pointed out by numerical experiments that nonlinear interactions can also induce inverse energy cascades by inducing resonant instabilities which transfer energy from higher to lower frequencies [43]. Originally, this phenomenon has been discovered analytically for rapidly-spinning BHs which can display turbulent gravitational behavior mediated by a parametric instability [44] and led to several studies regarding turbulence behaviour in gravitational wave physics [45–51].

In this paper we take a step further towards the study of the turbulent behaviour of QNMs, analyzing the case of the Schwarzschild BH. In particular, we investigate how small disturbances of a Schwarzschild BH redistribute energy across scalar modes and can initiate turbulence-like cascades. By applying the so-called van der Pol–Krylov–Bogoliubov averaging technique, we obtain a set of coupled mode equations capturing near-resonant couplings between neighboring angular multipoles. Our analysis contrasts two pathways to

instability: mixing at the difference frequency between adjacent modes, and a diagonal self-modulation mechanism akin to a Mathieu-type resonance. In the limit of large multipole indices (the eikonal regime), we will find that the difference-frequency mechanism prevails, producing a unidirectional flow of energy from higher to lower frequencies.

The paper is organized as follows. In section 2 we describe the dynamics of a massless scalar field subject to a monochromatic driver and study the two-mode reduction in section 3. Section 4 is dedicated to the higher-order instability. Finally, section 5 offers our conclusions.

2 Massless scalar on Perturbed Schwarzschild

Let us consider a massless scalar field propagating in a Schwarzschild spacetime, perturbed by an even-parity, axisymmetric quadrupole fluctuation (Zerilli field) of the metric. We choose a scalar field to avoid problems with gauge invariance arising beyond linear perturbation theory. The latter is a time-periodic field that acts as a “pump” or “driver” (to borrow the terminology from nonlinear optics [52, 53]) and modulates the parameters of the system while transfers energy to secondary (daughter or “idler”) modes from the primary (the parent or the “signal”) mode. As we will see below, the dynamics is of a time-dependent system that exhibits parametric resonance between a parent scalar mode of angular index ℓ and a daughter mode of index $\ell - 2$, driven by the $L = 2$, $M = 0$ gravitational pump at frequency Ω . In particular, we will expand the scalar in QNM radial functions, and by projecting the perturbed wave equation onto the QNM basis, we will isolate the two-mode truncation that exhibits the resonance tongue.

The Schwarzschild metric is written in standard Schwarzschild coordinates as

$$ds^2 = g_{\mu\nu}^{(0)} dx^\mu dx^\nu = -f dt^2 + f^{-1} dr^2 + r^2 (d\theta^2 + \sin^2 \theta d\phi^2), \quad f(r) = 1 - \frac{2M}{r}. \quad (2.1)$$

The perturbed metric is then $g_{\mu\nu} = g_{\mu\nu}^{(0)} + \varepsilon h_{\mu\nu}$, where $\varepsilon \ll 1$ is a bookkeeping small parameter and the even-parity, axisymmetric quadrupolar perturbation $h_{\mu\nu}$ is taken in Regge–Wheeler gauge to be

$$h_{\mu\nu} = \begin{pmatrix} f H_0 & H_1 & 0 & 0 \\ H_1 & f^{-1} H_2 & 0 & 0 \\ 0 & 0 & r^2 K & 0 \\ 0 & 0 & 0 & r^2 \sin^2 \theta K \end{pmatrix} Y_{20}(\theta, \phi). \quad (2.2)$$

The functions $H_0(r, t)$, $H_1(r, t)$, $H_2(r, t)$, $K(r, t)$ are determined algebraically by the Zerilli master field $Z_{20}(t, r)$. We consider a monochromatic QNM driver, with QNM frequency Ω

$$Z_{20}(t, r) = \text{Re} [\mathcal{Z}(r) e^{-i\Omega t}],$$

and, hence, each of H_i and K are of the same form, i.e.,

$$H_i(t, r) = \text{Re} [\hat{H}_i(r) e^{-i\Omega t}], \quad K(t, r) = \text{Re} [\hat{K}(r) e^{-i\Omega t}]. \quad (2.3)$$

The equation now for a massless scalar Φ on the perturbed Schwarzschild spacetime with metric $g_{\mu\nu} = g_{\mu\nu}^{(0)} + \varepsilon h_{\mu\nu}$ is written as

$$\square_g \Phi = \square_{g^{(0)}} \Phi - \varepsilon h^{ab} \nabla_a \nabla_b \Phi - \varepsilon \left(\nabla^a h_a{}^b - \frac{1}{2} \nabla^b h \right) \nabla_b \Phi = 0, \quad (2.4)$$

where indices are raised with $g^{(0)}$ and $h = h^a_a$.

Let $\{u_{\ell n}(r)\}$ denote the standard Schwarzschild scalar QNMs with azimuthal angular number ℓ and overtone n . They solve the equation

$$\partial_{r_*}^2 u_{\ell m} + \left(\omega_{\ell n}^2 - V_\ell(r)\right) u_{\ell m} = 0 \quad (2.5)$$

with the usual ingoing and outgoing boundary conditions at horizon and spatial infinity, respectively,

$$\begin{aligned} u_{\ell n} &\sim e^{-i\omega_{\ell n} r_*}, & (r_* \rightarrow -\infty), \\ u_{\ell n} &\sim e^{+i\omega_{\ell n} r_*}, & (r_* \rightarrow +\infty), \end{aligned} \quad (2.6)$$

whereas the scalar potential is

$$V_\ell(r) = f \left(\frac{\ell(\ell+1)}{r^2} + \frac{2M}{r^3} \right). \quad (2.7)$$

Although QNMs are non-renormalizable [54], following Green-Hollands-Zimmerman (GHZ) [55, 56], we may introduce in the space of (radial) solutions a conserved, symmetric bilinear form $\langle\langle \cdot, \cdot \rangle\rangle$ which is defined by a contour-renormalized Wronskian pairing such that

$$\langle\langle u_{\ell n}, u_{\ell' n'} \rangle\rangle = \mathcal{N}_{\ell n} \delta_{\ell\ell'} \delta_{nn'}, \quad \mathcal{N}_{\ell n} \neq 0, \quad (2.8)$$

and the QNM excitation coefficients are precisely the projections with respect to $\langle\langle \cdot, \cdot \rangle\rangle$. Specifically, one may take

$$\langle\langle u, v \rangle\rangle = \int_{\Gamma} u(r_*) v(r_*) dr_*, \quad (2.9)$$

where the integration path Γ is rotated into the complex r_* -plane so that the QNM asymptotics are integrable [55, 56]. In the following, we will only need the orthogonality of the QNMs with respect to the GHZ bilinear form and not the particular representation of the integral in (2.9).

We proceed by expanding the scalar Φ in the spherical harmonic basis as

$$\Phi(t, r, \theta, \phi) = \sum_{\ell m} \frac{\psi_{\ell m}(t, r)}{r} Y_{\ell m}(\theta, \phi). \quad (2.10)$$

We may now express the mode functions $\psi_{\ell m}(t, r)$ in terms of the QNMs of the corresponding problem on the exact (unperturbed) Schwarzschild spacetime. Keeping, for simplicity, only the fundamental overtone $n = 0$ in each ℓ , we may write

$$\psi_{\ell m}(t, r) = A_{\ell m}(t) u_\ell(r). \quad (2.11)$$

Then, the massless scalar equation (2.4) on the perturbed Schwarzschild spacetime, after separating the spherical harmonics $Y_{\ell m}$, multiplying with u_ℓ and GHZ-project, is written as

$$\langle\langle u_\ell, u_\ell \rangle\rangle \ddot{A}_{\ell m} + \langle\langle u_\ell, \omega_\ell^2 u_\ell \rangle\rangle A_{\ell m} + \varepsilon \sum_{\ell' m'} \langle\langle u_\ell, \mathcal{D}_{\ell\ell'}[h(t), u_{\ell'}] \rangle\rangle \mathcal{A}_{\ell m; \ell' m'}^{(20;0)} A_{\ell' m'} = 0. \quad (2.12)$$

Here $\mathcal{D}_{\ell\ell'}$ is the radial operator proportional to ε in Eq. (2.4). In addition, $\mathcal{A}_{\ell m; \ell' m'}^{(20;0)}$ is the purely angular Wigner factor for the even-parity, axisymmetric $L = 2, M = 0$ driver,

$$\mathcal{A}_{\ell m; \ell' m'}^{(20;0)} = \sqrt{\frac{5(2\ell+1)(2\ell'+1)}{4\pi}} \begin{pmatrix} \ell & 2 & \ell' \\ 0 & 0 & 0 \end{pmatrix} \begin{pmatrix} \ell & 2 & \ell' \\ -m & 0 & m' \end{pmatrix}, \quad (2.13)$$

so that axisymmetry enforces $m' = m$ and $\ell' = \ell, \ell \pm 2$. Using (2.8) and defining $\mathcal{N}_\ell = \langle\langle u_\ell, u_\ell \rangle\rangle$, we find, after dividing (2.12) by \mathcal{N}_ℓ , the equation

$$\ddot{A}_{\ell m} + \omega_\ell^2 A_{\ell m} + \varepsilon \sum_{\ell' m'} \mathcal{M}_{\ell m; \ell' m'}(t) A_{\ell' m'} = 0, \quad (2.14)$$

where the coupling coefficients are

$$\mathcal{M}_{\ell m; \ell' m'}(t) = \frac{\langle\langle u_\ell, \mathcal{D}_{\ell \ell'}[h(t), u_{\ell'}] \rangle\rangle}{\mathcal{N}_\ell} \mathcal{A}_{\ell m; \ell' m'}^{(20;0)}. \quad (2.15)$$

We may further define the quantities

$$q_\ell = \frac{\langle\langle u_\ell, \mathcal{D}_{\ell \ell}[\hat{H}_i, u_\ell] \rangle\rangle}{\mathcal{N}_\ell} G_{\ell \ell}, \quad c_\ell^\pm = \frac{\langle\langle u_\ell, \mathcal{D}_{\ell, \ell \pm 2}[\hat{H}_i, u_{\ell \pm 2}] \rangle\rangle}{\mathcal{N}_\ell} G_{\ell, \ell \pm 2}, \quad (2.16)$$

where

$$G_{\ell \ell'} = \mathcal{A}_{\ell 0; \ell' 0}^{(20;0)} = \sqrt{\frac{5(2\ell+1)(2\ell'+1)}{4\pi}} \begin{pmatrix} \ell & 2 & \ell' \\ 0 & 0 & 0 \end{pmatrix}^2. \quad (2.17)$$

Then, the projected chain turns out to be

$$\begin{aligned} \ddot{A}_\ell + \omega_\ell^2 A_\ell + \varepsilon q_\ell e^{\Omega_I t} \cos(\Omega_R t) A_\ell + \\ + \varepsilon c_\ell^+ e^{\Omega_I t} \cos(\Omega_R t) A_{\ell+2} + \varepsilon c_\ell^- e^{\Omega_I t} \cos(\Omega_R t) A_{\ell-2} = 0, \end{aligned} \quad (2.18)$$

where we have assumed a monochromatic Zerilli pump $H_i(t, r) = \text{Re}[\hat{H}_i(r)e^{-i\Omega t}]$, with $\Omega = \Omega_R + i\Omega_I$, ($\Omega_I < 0$).

3 Two-mode reduction

To proceed, let us truncate the GHZ-projected chain (2.18) to a parent-daughter pair $(\ell, \ell-2)$. The truncated amplitude system is then written as

$$\begin{aligned} \ddot{A}_\ell + \omega_\ell^2 A_\ell + \varepsilon q_\ell e^{\Omega_I t} \cos(\Omega_R t) A_\ell + \varepsilon c_\ell^- e^{\Omega_I t} \cos(\Omega_R t) A_{\ell-2} = 0, \\ \ddot{A}_{\ell-2} + \omega_{\ell-2}^2 A_{\ell-2} + \varepsilon q_{\ell-2} e^{\Omega_I t} \cos(\Omega_R t) A_{\ell-2} + \varepsilon c_{\ell-2}^+ e^{\Omega_I t} \cos(\Omega_R t) A_\ell = 0. \end{aligned} \quad (3.1)$$

In order to derive the coupled-mode equations and the growth rates near resonances from the system of Eqs (3.1), we will employ the van der Pol–Krylov–Bogoliubov averaging method, where slowly varying envelopes are introduced and subsequently, an averaging over the fast phase is performed [57]. Under the averaging (or rotating-wave approximation), only terms whose phases vary slowly survive,¹ Therefore, we introduce the narrow-band complex envelopes $a_\ell(t)$ such that

$$\begin{aligned} A_\ell(t) &= a_\ell(t) e^{-i\omega_\ell^R t} + a_\ell^*(t) e^{+i\omega_\ell^R t}, \\ A_{\ell-2}(t) &= a_{\ell-2}(t) e^{-i\omega_{\ell-2}^R t} + a_{\ell-2}^*(t) e^{+i\omega_{\ell-2}^R t}. \end{aligned} \quad (3.2)$$

¹In fact, one averages the equation over time windows T such that $\omega_\ell T \gg 1$ while $|\Delta_\ell|T = \mathcal{O}(1)$. Rapidly oscillating pieces integrate to zero to leading order in $1/(\omega_\ell T)$.

with the slow-variation conditions

$$|\dot{a}_\ell| \ll \omega_\ell^R |a_\ell|, \quad |\ddot{a}_\ell| \ll \omega_\ell^R |\dot{a}_\ell|, \quad (3.3)$$

and $\omega_\ell = \omega_\ell^R - i\alpha_\ell$ with $\alpha_\ell \ll \omega_\ell^R$. Substituting (3.2) into (3.1) and keeping only near-stationary phase terms, we obtain, after averaging over the fast carriers, the first-order envelope system

$$\dot{a}_\ell = -\alpha_\ell a_\ell - \frac{i\varepsilon}{4\omega_\ell^R} q_\ell e^{\Omega_I t} a_\ell e^{+i\sigma_\ell t} - \frac{i\varepsilon}{2\omega_\ell^R} c_\ell^- e^{\Omega_I t} a_{\ell-2} e^{+i\Delta_\ell t}, \quad (3.4)$$

$$\dot{a}_{\ell-2} = -\alpha_{\ell-2} a_{\ell-2} - \frac{i\varepsilon}{4\omega_{\ell-2}^R} q_{\ell-2} e^{\Omega_I t} a_{\ell-2} e^{+i\sigma_{\ell-2} t} - \frac{i\varepsilon}{2\omega_{\ell-2}^R} c_{\ell-2}^+ e^{\Omega_I t} a_\ell e^{-i\Delta_\ell t}. \quad (3.5)$$

where $\alpha_\ell = -\text{Im } \omega_\ell > 0$ and the detunings are

$$\Delta_\ell = \Omega_R - (\omega_\ell^R - \omega_{\ell-2}^R), \quad \sigma_\ell = \Omega_R - 2\omega_\ell^R. \quad (3.6)$$

Equations (3.4)–(3.5) show explicitly the two near-resonant channels: (i) the difference-frequency or 3-wave mixing ($\Delta_\ell \approx 0$, off-diagonal terms) and (ii) the diagonal Mathieu self-modulation ($\sigma_\ell \approx 0$, diagonal terms). Their instability regions and growth rates will be used determined below

3.1 Off-diagonal, three-wave mixing channel

The first near-resonant channel arises from the off-diagonal difference-frequency terms from c_ℓ^\pm (3-wave mixing). In this channel only phases that are nearly stationary with detuning

$$\Delta_\ell = \Omega_R - (\omega_\ell^R - \omega_{\ell-2}^R) \approx 0. \quad (3.7)$$

survive the van der Pol–Krylov–Bogoliubov averaging. Therefore, in this channel, the slow-envelope equations are

$$\dot{a}_\ell = -\alpha_\ell a_\ell - \frac{i\varepsilon}{2\omega_\ell^R} c_\ell^- e^{\Omega_I t} a_{\ell-2} e^{+i\Delta_\ell t}, \quad (3.8)$$

$$\dot{a}_{\ell-2} = -\alpha_{\ell-2} a_{\ell-2} - \frac{i\varepsilon}{2\omega_{\ell-2}^R} c_{\ell-2}^+ e^{\Omega_I t} a_\ell e^{-i\Delta_\ell t}, \quad (3.9)$$

where, the off-diagonal coefficients are c_ℓ^- and $c_{\ell-2}^+$ are

$$\begin{aligned} c_\ell^- &= \frac{G_{\ell,\ell-2}}{\mathcal{N}_\ell} \sum_{X \in \{tt, tr, rr, \theta\theta, \phi\phi\}} \mathcal{J}_{\ell,\ell-2}^{(X)}, \\ c_{\ell-2}^+ &= \frac{G_{\ell-2,\ell}}{\mathcal{N}_{\ell-2}} \sum_{X \in \{tt, tr, rr, \theta\theta, \phi\phi\}} \mathcal{J}_{\ell-2,\ell}^{(X)}, \end{aligned} \quad (3.10)$$

where the angular factor $G_{\ell,\ell-2}$ is given by

$$G_{\ell,\ell-2} = \frac{15}{2\pi} \frac{\ell^2(\ell-1)^2}{(2\ell)(2\ell-1)(2\ell-2)}, \quad (3.11)$$

\mathcal{N}_ℓ is the GHZ norm ($\mathcal{N}_\ell = \langle\langle u_\ell, u_\ell \rangle\rangle$), and

$$\begin{aligned}\mathcal{J}_{\ell\ell'}^{(tt)} &= \langle\langle u_\ell, f^{-1}\hat{H}_0(-\omega_{\ell'}^2)u_{\ell'} + \frac{1}{2}f^{-1}(-i\Omega)(-i\omega_{\ell'})\hat{H}_0u_{\ell'} \rangle\rangle, \\ \mathcal{J}_{\ell\ell'}^{(tr)} &= \langle\langle u_\ell, 2\hat{H}_1(i\omega_{\ell'})u_{\ell'} + \left((-i\Omega)\hat{H}_1 + \frac{f'}{f}\hat{H}_1\right)u_{\ell'} \rangle\rangle, \\ \mathcal{J}_{\ell\ell'}^{(rr)} &= \langle\langle u_\ell, f\hat{H}_2u_{\ell'}'' + \left(\frac{f'}{2}\hat{H}_2 + \frac{f}{2}\hat{H}_2'\right)u_{\ell'} \rangle\rangle,\end{aligned}\tag{3.12}$$

$$\begin{aligned}\mathcal{J}_{\ell\ell'}^{(\theta\theta)} &= \langle\langle u_\ell, \frac{\hat{K}}{r^2}\ell'(\ell'+1)u_{\ell'} + \frac{\hat{K}'}{r}u_{\ell'} + \frac{(-i\Omega)\hat{K}}{fr}(i\omega_{\ell'})u_{\ell'} \rangle\rangle, \\ \mathcal{J}_{\ell\ell'}^{(\theta\phi)} &= \mathcal{J}_{\ell\ell'}^{(\phi\phi)}.\end{aligned}\tag{3.13}$$

By parametrizing a_ℓ and $a_{\ell-2}$ by new narrow envelopes b_ℓ and $b_{\ell-2}$ defined by

$$a_\ell = b_\ell = \rho^{-1}e^{i\theta}b_\ell e^{i\Delta_\ell t/2}, \quad a_{\ell-2} = \rho e^{-i\theta}b_{\ell-2}e^{-i\Delta_\ell t/2},\tag{3.14}$$

where

$$\rho = \sqrt{\frac{\omega_\ell |c_{\ell-2}^+|}{\omega_{\ell-2} |c_\ell^+|}}, \quad \theta = \frac{1}{2}(\pi - \arg c_{\ell-2}^+ - \arg c_\ell^-),\tag{3.15}$$

we find that Eqs (3.8) and (3.9) are written as the linear 2×2 system

$$\begin{pmatrix} \dot{b}_\ell \\ \dot{b}_{\ell-2} \end{pmatrix} = \underbrace{\begin{pmatrix} -\alpha_\ell - i\frac{\Delta_\ell}{2} & i g(t) \\ -i g(t) & -\alpha_{\ell-2} + i\frac{\Delta_\ell}{2} \end{pmatrix}}_{= \mathcal{M}_d(t)} \begin{pmatrix} b_\ell \\ b_{\ell-2} \end{pmatrix}.\tag{3.16}$$

with

$$g(t) = g_0 e^{\Omega_I t}, \quad g_0 = \frac{\varepsilon}{2} \sqrt{\frac{|c_\ell^- c_{\ell-2}^+|}{\omega_\ell^R \omega_{\ell-2}^R}},\tag{3.17}$$

If $|\Omega_I|$ is small compared to all oscillation or damping rates, the growth can be determined adiabatically by treating $g(t)$ as frozen. The instantaneous Floquet exponents are the eigenvalues of $\mathcal{M}_d(t)$,

$$\lambda_\pm(t) = -\frac{\alpha_\ell + \alpha_{\ell-2}}{2} \pm \frac{1}{2} \sqrt{4g(t)^2 + (a_\ell - a_{\ell-2})^2 - \Delta_\ell^2 + 2i(a_\ell - a_{\ell-2})\Delta_\ell}.\tag{3.18}$$

Instability occurs whenever the eigenvalues have positive real part, i.e.,

$$\text{Re}(\lambda_+) > 0.\tag{3.19}$$

$(\alpha_\ell + \alpha_{\ell-2})/2$, where

$$\begin{aligned}\text{Re}(\lambda_+) &= -\frac{\alpha_\ell + \alpha_{\ell-2}}{2} + \frac{1}{2\sqrt{2}} \left\{ \left[\left(4g(t)^2 + (a_\ell - a_{\ell-2})^2 - \Delta_\ell^2 \right)^2 + 4(a_\ell - a_{\ell-2})^2 \Delta_\ell^2 \right]^{1/2} \right. \\ &\quad \left. + 4g(t)^2 + (a_\ell - a_{\ell-2})^2 - \Delta_\ell^2 \right\}^{1/2}\end{aligned}\tag{3.20}$$

For balanced damping with $\alpha_\ell = \alpha_{\ell-2} = \alpha$, we find that instability sets in ($\text{Re } \lambda_+ = 0$) for the threshold value of g

$$g_{\text{thr}} = \sqrt{\alpha^2 + \frac{\Delta_\ell^2}{4}}. \quad (3.21)$$

Expressing g through the physical modulation depth ε gives

$$\varepsilon_{\text{thr}}(\Omega_R, t) = e^{-\Omega_I t} \sqrt{\frac{\omega_\ell^R \omega_{\ell-2}^R}{|c_\ell^- c_{\ell-2}^+|}} \sqrt{4\alpha^2 + \left[\Omega_R - (\omega_\ell^R - \omega_{\ell-2}^R)\right]^2}. \quad (3.22)$$

It is convenient to factor out the unknown coupling normalization and define the normalized threshold

$$\tilde{\varepsilon}_{\text{thr}}(\Omega_R) = \frac{\varepsilon_{\text{thr}}}{2} \sqrt{\frac{|c_\ell^- c_{\ell-2}^+|}{2\omega_\ell^R \omega_{\ell-2}^R}} e^{\Omega_I t} = \frac{1}{2} \sqrt{4\alpha^2 + \left[\Omega_R - (\omega_\ell^R - \omega_{\ell-2}^R)\right]^2}. \quad (3.23)$$

The difference-frequency resonance tongue for large ℓ is plotted in Fig. 1.

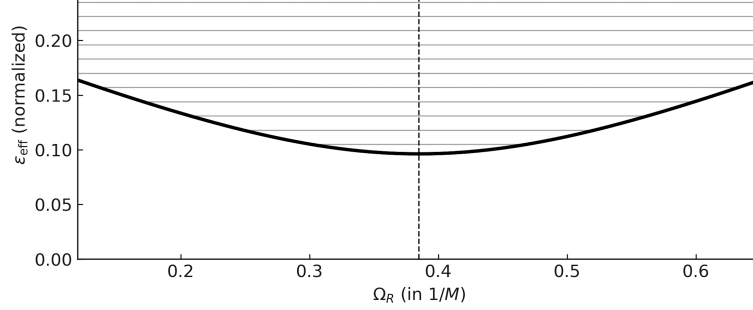


Figure 1: Arnold instability tongue for the difference-frequency (three-wave) channel. The solid curve is the normalized threshold $\tilde{\varepsilon}_{\text{thr}}(\Omega_R) = \sqrt{\alpha^2 + \frac{1}{4}[\Omega_R - (\omega_\ell^R - \omega_{\ell-2}^R)]^2}$, and the horizontally hatched region denotes instability ($\tilde{\varepsilon} \geq \tilde{\varepsilon}_{\text{thr}}$). The vertical dashed line marks the resonance center $\Omega_R = \omega_\ell^R - \omega_{\ell-2}^R$. For this plot we used the eikonal spacings $\omega_\ell^R - \omega_{\ell-2}^R = 2\omega_c$ and $\alpha = \omega_c/2$, where $\omega_c = 1/3\sqrt{3}M$. In practice, even low ℓ give the same Arnold tongues so the plot changes only by a small horizontal shift with a new minimum and a vertical adjustment. For example, even $\ell = 6$ scalar QNMs are already very close to eikonal values.

We note also that three-wave mixing appears in rotating stars arising from quadratic mode couplings. In this case, quadratic perturbations couple the unstable f -mode to otherwise stable daughter modes and when near-resonance conditions are met, three-wave mixing triggers parametric resonance, redistributing energy among the modes and saturating the f -mode amplitude [58, 59].

3.2 Diagonal Mathieu channel

The second near-resonant instability arises from the diagonal Mathieu, self-parametric channel. In this case, the diagonal modulation within the narrow-band approximation of Eqs (3.4) and (3.5) turns out to be

$$\begin{aligned} \dot{a}_\ell &= -\alpha_\ell a_\ell - \frac{i\varepsilon}{4\omega_\ell^R} q_\ell e^{\Omega_I t} a_\ell^* e^{+i\sigma_\ell t}, \\ \dot{a}_\ell^* &= -\alpha_\ell a_\ell^* + \frac{i\varepsilon}{4\omega_\ell^R} q_\ell^* e^{\Omega_I t} a_\ell e^{-i\sigma_\ell t}, \quad \sigma_\ell = 2\omega_\ell - \Omega_R \simeq 0. \end{aligned} \quad (3.24)$$

We may now define new envelopes b_ℓ and b_ℓ^* such that

$$a_\ell = b_\ell e^{+i\sigma_\ell t/2}, \quad a_\ell^* = b_\ell^* e^{-i\sigma_\ell t/2} \quad (3.25)$$

and let $p(t) = \frac{\varepsilon|q_\ell|}{4\omega_\ell} e^{\Omega_I t}$. Then, Eq. (3.24) is written as

$$\begin{pmatrix} \dot{b}_\ell \\ \dot{b}_\ell^* \end{pmatrix} = \underbrace{\begin{pmatrix} -\alpha_\ell - i\sigma_\ell/2 & -i p(t) e^{i\phi_\ell} \\ +i p(t) e^{-i\phi_\ell} & -\alpha_\ell + i\sigma_\ell/2 \end{pmatrix}}_{\mathcal{M}_\sigma(t)} \begin{pmatrix} b_\ell \\ b_\ell^* \end{pmatrix}, \quad (3.26)$$

where $\phi = \arg q_\ell$. The eigenvalues of the matrix $\mathcal{M}_\sigma(t)$ are

$$\lambda_\pm = -\alpha_\ell \pm \frac{1}{2} \sqrt{4p(t)^2 - \sigma_\ell^2}. \quad (3.27)$$

Then, instability occurs whenever $\text{Re}(\lambda_+) > 0$, which is the case for

$$p(t) > \frac{1}{2} \sqrt{4\alpha_\ell^2 + \sigma_\ell^2}. \quad (3.28)$$

In other words, instability is set in for the threshold value of $p(t)$

$$p_{\text{th}}(t) = \frac{1}{2} \sqrt{4\alpha_\ell^2 + (2\omega_\ell^R - \Omega_R)^2}, \quad (3.29)$$

which corresponds to the threshold for physical modulation depth ε

$$\varepsilon_{\text{th}}(\Omega, t) = e^{-\Omega_I t} \frac{2\omega_\ell^R}{|q_\ell|} \sqrt{4\alpha_\ell^2 + (2\omega_\ell^R - \Omega_R)^2}. \quad (3.30)$$

Again, it is convenient to factor out the unknown coupling normalization and define the normalized threshold

$$\tilde{\varepsilon}_{\text{th}}(\Omega_R, \omega_\ell^R) = \frac{\varepsilon_{\text{th}}|q_\ell|}{4\omega_\ell} e^{\Omega_I t} = \frac{1}{2} \sqrt{4\alpha_\ell^2 + (2\omega_\ell^R - \Omega_R)^2}. \quad (3.31)$$

Therefore the Mathieu instability is centered at $\Omega_R = 2\omega_\ell^R$ with boundary $\tilde{\varepsilon}_{\text{th}}$. At exact tuning ($\sigma_\ell = 0$) one has $\tilde{\varepsilon}_{\text{th}} = \alpha_\ell$ (e.g. $p(0) > \alpha_\ell$ for a decaying pump $\Omega_I < 0$) to obtain net amplification within the pump lifetime. The Arnold tongue for the Mathieu channel centered at $\mu = 1$ is plotted in Fig. (2). One may notice that there are additional tongues centered in Fig. (2) for $\mu = \frac{1}{2}, \frac{1}{3}, \dots$, which we will explain below.

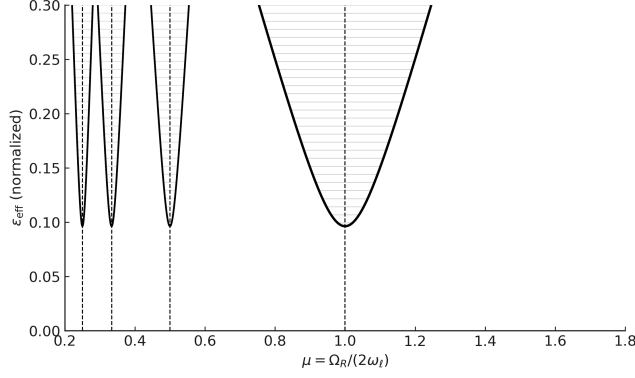


Figure 2: Mathieu-type parametric-instability map in the scaled plane $\mu = \Omega_R/(2\omega_\ell)$ and $\varepsilon_{\text{eff}} = \varepsilon|q_\ell|/(4\omega_\ell)$. Black curves are the instability boundaries; horizontal grey lines indicate the unstable region. The primary lobe is centered at $\mu = 1$; higher-order tongues at $\mu = \frac{1}{2}, \frac{1}{3}, \frac{1}{4}$ are shown narrower, as expected from higher-order averaging. Vertical dashed lines mark the tongue centers.

We should stress here that the instabilities we described above is in fact a transient instability. The reason is that the matrices $\mathcal{M}_d(t)$ and $\mathcal{M}_\sigma(t)$ are functions of time. For the particular $\mathcal{M}_\sigma(t)$ for example, the positivity of the maximum eigenvalue, although it implies transient instability, it does not imply global time instability. In fact, the solution of the system of Eq. (3.26) is bounded by

$$b_\ell(t) < b_\ell(0)e^{\int_0^t (-\alpha_\ell - |p(\tau)|)d\tau}. \quad (3.32)$$

Then, it is easy to verify that transient growth exists up to a time scale

$$t_s = \frac{1}{|\Omega_I|} \ln \left(\frac{p(0)}{\alpha_\ell} \right), \quad (3.33)$$

after which we end up in exponential decay. In other words, there is no long-time parametric divergence with a decaying pump ($e^{\Omega_I t}$) since only bounded transient growth is possible.

4 Higher-order instability

These tongues are originated from nonlinear GR as we will explain below. In our setup the scalar amplitude A_ℓ experiences a parametric modulation because the background metric is not strictly stationary: it is weakly time-periodic with frequency Ω_R due to an $L = 2, M = 0$ pump. At first order in the metric amplitude (or ε), we found a single harmonic proportional to $\cos \Omega_R t$ in the coefficients of the scalar master equation. At higher orders of the Einstein perturbation expansion, new harmonics $n\Omega_R$ necessarily appear, and these are precisely the harmonics that generate the tongues centered at $\mu = \Omega_R/(2\omega_\ell^R) = 1/n$.

In order to find out here the higher harmonics $n\Omega_R$ come from, let us recall that the metric is expanded as

$$g_{ab} = g_{ab}^{(0)} + \varepsilon h_{ab}^{(1)} + \varepsilon^2 h_{ab}^{(2)} + \varepsilon^3 h_{ab}^{(3)} + \dots, \quad (4.1)$$

with $g_{ab}^{(0)}$ the background Schwarzschild metric and $h_{ab}^{(1)}(t, \mathbf{x}) = \text{Re}[\hat{H}_{ab}^{(1)}(\mathbf{x}) e^{-i\Omega_R t}]$ the first-order pump with $L = 2, M = 0$. Einstein's equations $E[g] = 0$ expand schematically as

$$\mathcal{E}[h^{(1)}] = 0, \quad (4.2)$$

$$\mathcal{E}[h^{(2)}] = S^{(2)}[h^{(1)}, h^{(1)}], \quad \mathcal{E}[h^{(3)}] = S^{(3)}[h^{(1)}, h^{(2)}] + \tilde{S}^{(3)}[h^{(1)}, h^{(1)}, h^{(1)}], \quad \text{etc.} \quad (4.3)$$

Here \mathcal{E} is the linearized Einstein operator about Schwarzschild, and $S^{(k)}$ are multilinear source functionals built from products of lower-order fields and their derivatives. Because $h^{(1)} \sim e^{-i\Omega_R t}$, the quadratic source contains harmonics

$$S^{(2)}[h^{(1)}, h^{(1)}] \sim \{(e^{-i\Omega_R t})^2, e^{-i\Omega_R t} e^{+i\Omega_R t}, (e^{+i\Omega_R t})^2\} = \{e^{-2i\Omega_R t}, 1, e^{+2i\Omega_R t}\}. \quad (4.4)$$

Thus, the second-order metric $h^{(2)}$ contains a component oscillating at $2\Omega_R$, as well as a constant component. At third order one similarly obtains $h^{(3)}$ with harmonics at $3\Omega_R$, and so on. Therefore the time-dependence of the effective coefficients in the scalar master equation inevitably involves a Fourier series, since Eq. (2.18) has the schematic form, up to k -th order,

$$\ddot{A}_\ell + \omega_\ell^2 A_\ell + \sum_{n=1}^k \sum_{|l-2n| \leq l \leq l+2n} \varepsilon^n C_{mn}^{(\ell)} e^{n\Omega_R t} \cos(n\Omega_R t) A_m = 0. \quad (4.5)$$

The appearance of $2n+1$ terms in Eq. (4.5) is due to the spherical harmonic relation

$$\underbrace{Y_{20} Y_{20} \cdots Y_{20}}_{n \text{ factors}} = \sum_{L \in \{0, 2, 4, \dots, 2n\}} c_L^{(n)} Y_{L0}. \quad (4.6)$$

Now, each harmonic $\cos(n\Omega_R t)$ acts as an n -th harmonic parametric driver. Consequently, in the self-modulation, A_ℓ satisfies

$$\ddot{A}_\ell + \omega_\ell^2 A_\ell + \left[\sum_{n=1}^k \varepsilon^n C_{\ell n}^{(\ell)} e^{n\Omega_R t} \cos(n\Omega_R t) \right] A_\ell = 0. \quad (4.7)$$

so that the near-resonant phase that survives averaging is $e^{i(2\omega_\ell^R - n\Omega_R)t}$, producing the standard Mathieu resonance condition

$$2\omega_\ell^R \approx n\Omega_R \quad \Longleftrightarrow \quad \mu = \frac{\Omega_R}{2\omega_\ell^R} \approx \frac{1}{n}, \quad n = 1, 2, 3, \dots \quad (4.8)$$

Hence, there are now Arnold tongues centered at $\mu = 1/n$, which are the ones depicted in Fig. (2). Importantly, the order in perturbation theory that first produces the n -th harmonic also sets the scaling of its strength. The amplitude of the n th harmonic is generically $\mathcal{O}(\varepsilon^n)$ in GR perturbation theory, which yields the shrinking of the higher tongues we see in Fig. 2.

The discussion above concerns the diagonal, self-modulation channel, where a_ℓ couples to its complex conjugate a_ℓ^* . In contrast, the difference-frequency (three-wave) channel couples a_ℓ and $a_{\ell-2}$ with a near-stationary phase $e^{i(\omega_\ell - \omega_{\ell-2} - \Omega_R)t}$, producing a single strong tongue centered at $\Omega_R \simeq \omega_\ell^R - \omega_{\ell-2}^R$ (which tends to $2\Omega_c$ in the eikonal limit). Additional comb-like tongues do not arise since for the n th harmonic we will have

$$\Omega_R = \frac{\omega_\ell^R - \omega_{\ell-2}^R}{n}. \quad (4.9)$$

Since, $\omega_\ell^R - \omega_{\ell-2}^R \approx 2\omega_c$, there is a single-tone pump Ω_R that satisfies (4.9) for a given n (taken to be the leading $n = 1$), so that $\Omega_R \approx 2\omega_c$. Therefore, no higher Arnold tongues appear in the three-wave channel.

A final comment concerns ε , which although it has been introduced as a bookkeeping parameter in first place, it has acquired physical meaning as the dimensionless pump amplitude. This is possible since if one rescales the pump as $\hat{H}_{ab} \rightarrow A \hat{H}_{ab}$ and simultaneously sets $\varepsilon \rightarrow 1$, all formulas are unchanged except that ε is replaced by the physical amplitude A . In practice, we either keep ε explicit and calculate ε_{thr} , or set $\varepsilon = 1$ and state the threshold directly as a condition on the pump amplitude (or on the norm of \hat{H}_{ab}) as A_{thr} . We have chosen the first option.

5 Conclusions

Nonlinear interactions of gravity generate a plethora of unexpected phenomena, rendering the detection of BH QNMs an unique occasion to learn about the properties of gravity. The nonlinear dynamics explored here shed also light on binary BH behavior. During merger, equal-mass circular systems primarily excite the $\ell = 2$ mode, with frequency increasing during inspiral. Our results, as well as the recent ones in the literature [60], seem to indicate that resonant interactions tend to preserve the lowest angular and frequency modes. This has important consequences from the observational side, e.g. on the perspective to detect the quadratic QNMs. Of course our results are based on the impact on a scalar probe, the next necessary step will be to generalize our findings to the gravitational degrees of freedom.

Acknowledgments

We would like to thank K. Kokkotas for illuminating discussions. A.R. acknowledges support from the Swiss National Science Foundation (project number CRSII5_213497).

References

- [1] E. Berti et al., *Black hole spectroscopy: from theory to experiment*, [2505.23895](#).
- [2] LIGO SCIENTIFIC, VIRGO collaboration, R. Abbott et al., *Tests of general relativity with binary black holes from the second LIGO-Virgo gravitational-wave transient catalog*, *Phys. Rev. D* **103** (2021) 122002, [[2010.14529](#)].
- [3] LIGO SCIENTIFIC, VIRGO, KAGRA collaboration, R. Abbott et al., *Tests of General Relativity with GWTC-3*, [2112.06861](#).
- [4] C. D. Capano, M. Cabero, J. Westerweck, J. Abedi, S. Kasta, A. H. Nitz et al., *Multimode Quasinormal Spectrum from a Perturbed Black Hole*, *Phys. Rev. Lett.* **131** (2023) 221402, [[2105.05238](#)].
- [5] E. Finch and C. J. Moore, *Searching for a ringdown overtone in GW150914*, *Phys. Rev. D* **106** (2022) 043005, [[2205.07809](#)].
- [6] M. Isi and W. M. Farr, *Revisiting the ringdown of GW150914*, [2202.02941](#).
- [7] R. Cotesta, G. Carullo, E. Berti and V. Cardoso, *Analysis of Ringdown Overtones in GW150914*, *Phys. Rev. Lett.* **129** (2022) 111102, [[2201.00822](#)].
- [8] H. Siegel, M. Isi and W. M. Farr, *Ringdown of GW190521: Hints of multiple quasinormal modes with a precessional interpretation*, *Phys. Rev. D* **108** (2023) 064008, [[2307.11975](#)].
- [9] E. Berti, V. Cardoso and C. M. Will, *On gravitational-wave spectroscopy of massive black holes with the space interferometer LISA*, *Phys. Rev. D* **73** (2006) 064030, [[gr-qc/0512160](#)].
- [10] I. Ota and C. Chirenti, *Overtones or higher harmonics? Prospects for testing the no-hair theorem with gravitational wave detections*, *Phys. Rev. D* **101** (2020) 104005, [[1911.00440](#)].

- [11] S. Bhagwat, X. J. Forteza, P. Pani and V. Ferrari, *Ringdown overtones, black hole spectroscopy, and no-hair theorem tests*, *Phys. Rev. D* **101** (2020) 044033, [[1910.08708](#)].
- [12] C. Pitte, Q. Baghi, M. Besançon and A. Petiteau, *Exploring tests of the no-hair theorem with LISA*, *Phys. Rev. D* **110** (2024) 104003, [[2406.14552](#)].
- [13] L. London, D. Shoemaker and J. Healy, *Modeling ringdown: Beyond the fundamental quasinormal modes*, *Phys. Rev. D* **90** (2014) 124032, [[1404.3197](#)].
- [14] K. Mitman et al., *Nonlinearities in Black Hole Ringdowns*, *Phys. Rev. Lett.* **130** (2023) 081402, [[2208.07380](#)].
- [15] M. H.-Y. Cheung et al., *Nonlinear Effects in Black Hole Ringdown*, *Phys. Rev. Lett.* **130** (2023) 081401, [[2208.07374](#)].
- [16] S. Ma, K. Mitman, L. Sun, N. Deppe, F. Hébert, L. E. Kidder et al., *Quasinormal-mode filters: A new approach to analyze the gravitational-wave ringdown of binary black-hole mergers*, *Phys. Rev. D* **106** (2022) 084036, [[2207.10870](#)].
- [17] J. Redondo-Yuste, G. Carullo, J. L. Ripley, E. Berti and V. Cardoso, *Spin dependence of black hole ringdown nonlinearities*, *Phys. Rev. D* **109** (2024) L101503, [[2308.14796](#)].
- [18] M. H.-Y. Cheung, E. Berti, V. Baibhav and R. Cotesta, *Extracting linear and nonlinear quasinormal modes from black hole merger simulations*, *Phys. Rev. D* **109** (2024) 044069, [[2310.04489](#)].
- [19] H. Zhu et al., *Nonlinear effects in black hole ringdown from scattering experiments: Spin and initial data dependence of quadratic mode coupling*, *Phys. Rev. D* **109** (2024) 104050, [[2401.00805](#)].
- [20] A. Kehagias, D. Perrone, A. Riotto and F. Riva, *Explaining nonlinearities in black hole ringdowns from symmetries*, *Phys. Rev. D* **108** (2023) L021501, [[2301.09345](#)].
- [21] D. Perrone, T. Barreira, A. Kehagias and A. Riotto, *Non-linear black hole ringdowns: An analytical approach*, *Nucl. Phys. B* **999** (2024) 116432, [[2308.15886](#)].
- [22] S. Ma and H. Yang, *Excitation of quadratic quasinormal modes for Kerr black holes*, *Phys. Rev. D* **109** (2024) 104070, [[2401.15516](#)].
- [23] P. Bourg, R. Panosso Macedo, A. Spiers, B. Leather, B. Bonga and A. Pound, *Quadratic quasi-normal mode dependence on linear mode parity*, [2405.10270](#).
- [24] B. Bucciotti, L. Juliano, A. Kuntz and E. Trincherini, *Quadratic Quasi-Normal Modes of a Schwarzschild Black Hole*, [2405.06012](#).
- [25] N. Khera, S. Ma and H. Yang, *Quadratic Mode Couplings in Rotating Black Holes and Their Detectability*, [2410.14529](#).
- [26] A. Kehagias and A. Riotto, *Nonlinear effects in black hole ringdown made simple: Quasinormal modes as adiabatic modes*, *Phys. Rev. D* **111** (2025) L041506, [[2411.07980](#)].
- [27] B. Bucciotti, V. Cardoso, A. Kuntz, D. Pereñíguez and J. Redondo-Yuste, *Ringdown nonlinearities in the eikonal regime*, [2501.17950](#).
- [28] P. Bourg, R. P. Macedo, A. Spiers, B. Leather, B. Béatrice and A. Pound, *Quadratic quasinormal modes at null infinity on a schwarzschild spacetime*, 2025.
- [29] J. Ben Achour and H. Roussille, *Quadratic perturbations of the Schwarzschild black hole: the algebraically special sector*, *JCAP* **07** (2024) 085, [[2406.08159](#)].
- [30] A. Kehagias and A. Riotto, *Nonlinear Tails of Gravitational Waves in Schwarzschild Black Hole Ringdown*, [2504.06224](#).
- [31] S. Ling, S. Shah and S. S. C. Wong, *Dynamical nonlinear tails in Schwarzschild black hole ringdown*, [2503.19967](#).

- [32] A. Kehagias and A. Riotto, *The AdS Perspective on the Nonlinear Tails in Black Hole Ringdown*, [2506.14475](#).
- [33] D. Perrone, A. Kehagias and A. Riotto, *Nonlinearities in Kerr black hole ringdown from the Penrose limit*, *JCAP* **10** (2025) 024, [[2507.01919](#)].
- [34] K. Fransen, D. Pereñíguez and J. Redondo-Yuste, *Perturbations of Plane Waves and Quadratic Quasinormal Modes on the Lightring*, [2509.03598](#).
- [35] A. Kehagias, D. Perrone and A. Riotto, *Non-linear Quasi-Normal Modes of the Schwarzschild Black Hole from the Penrose Limit*, [2503.09350](#).
- [36] A. Kehagias, D. Perrone and A. Riotto, *Nonlinearities of Schwarzschild Black Hole Head-on Collisions*, [2508.17993](#).
- [37] A. Iannicari, L. Lo Bianco and A. Riotto, *The nonlinear tails in black hole ringdown: the scattering perspective*, *JCAP* **10** (2025) 062, [[2507.17732](#)].
- [38] J. Singh and V. Suneeta, *Computing nonlinearity ratios using second order black hole perturbation theory*, [2512.00943](#).
- [39] M. Lagos, T. Andrade, J. Rafecas-Ventosa and L. Hui, *Black hole spectroscopy with nonlinear quasinormal modes*, *Phys. Rev. D* **111** (2025) 024018, [[2411.02264](#)].
- [40] S. Yi, A. Kuntz, E. Barausse, E. Berti, M. H.-Y. Cheung, K. Kritos et al., *Nonlinear quasinormal mode detectability with next-generation gravitational wave detectors*, *Physical Review D* **109** (June, 2024) .
- [41] Y. Qiu, X. J. Forteza and P. Mourier, *Linear versus nonlinear modeling of black hole ringdowns*, *Phys. Rev. D* **109** (Mar, 2024) 064075.
- [42] C. Shi, Q. Zhang and J. Mei, *On the detectability and resolvability of quasi-normal modes with space-based gravitational wave detectors*, 2024.
- [43] S. Ma, M. Giesler, V. Varma, M. A. Scheel and Y. Chen, *Universal features of gravitational waves emitted by superkick binary black hole systems*, *Phys. Rev. D* **104** (2021) 084003, [[2107.04890](#)].
- [44] H. Yang, A. Zimmerman and L. Lehner, *Turbulent Black Holes*, *Phys. Rev. Lett.* **114** (2015) 081101, [[1402.4859](#)].
- [45] S. Galtier and S. V. Nazarenko, *Turbulence of Weak Gravitational Waves in the Early Universe*, *Phys. Rev. Lett.* **119** (2017) 221101, [[1703.09069](#)].
- [46] S. Galtier, S. V. Nazarenko, É. Buchlin and S. Thalabard, *Nonlinear Diffusion Models for Gravitational Wave Turbulence*, *Physica D* **390** (2019) 84–88, [[1809.07623](#)].
- [47] G. Benomio, A. Cárdenas-Avendaño, F. Pretorius and A. Sullivan, *Turbulence for spacetimes with stable trapping*, *Phys. Rev. D* **111** (2025) 104037, [[2411.17445](#)].
- [48] C. Iuliano, S. Hollands, S. R. Green and P. Zimmerman, *Extremal black hole weather*, *Phys. Rev. D* **111** (2025) 124038, [[2412.02821](#)].
- [49] P. Figueras and L. Rossi, *Non-linear instability of slowly rotating Kerr-AdS black holes*, *JHEP* **06** (2025) 107, [[2311.14167](#)].
- [50] H. Krynicky, J. Wu and E. R. Most, *Toward a Theory of Gravitational Wave Turbulence*, [2509.19769](#).
- [51] N. Siemonsen, *Weakly turbulent saturation of the nonlinear scalar ergoregion instability*, [2510.07467](#).
- [52] B. E. A. Saleh and M. C. Teich, *Fundamentals of Photonics*. Wiley, Hoboken, NJ, 2 ed., 2007.
- [53] R. W. Boyd, *Nonlinear Optics*. Academic Press, Burlington, MA, 2008.

- [54] K. D. Kokkotas and B. G. Schmidt, *Quasinormal modes of stars and black holes*, *Living Rev. Rel.* **2** (1999) 2, [[gr-qc/9909058](#)].
- [55] S. R. Green, S. Hollands, L. Sberna, V. Toomani and P. Zimmerman, *Conserved currents for a Kerr black hole and orthogonality of quasinormal modes*, *Phys. Rev. D* **107** (2023) 064030, [[2210.15935](#)].
- [56] E. Cannizzaro, L. Sberna, S. R. Green and S. Hollands, *Relativistic Perturbation Theory for Black-Hole Boson Clouds*, *Phys. Rev. Lett.* **132** (2024) 051401, [[2309.10021](#)].
- [57] A. H. Nayfeh, *Perturbation Methods*. Wiley-Interscience, New York, 1973.
- [58] P. Pnigouras and K. D. Kokkotas, *Saturation of the f -mode instability in neutron stars: Theoretical framework*, *Phys. Rev. D* **92** (2015) 084018, [[1509.01453](#)].
- [59] P. Pnigouras and K. D. Kokkotas, *Saturation of the f -mode instability in neutron stars: II. Applications and results*, *Phys. Rev. D* **94** (2016) 024053, [[1607.03059](#)].
- [60] S. Ma, L. Lehner, H. Yang, L. E. Kidder, H. P. Pfeiffer and M. A. Scheel, *Emergent Turbulence in Nonlinear Gravity*, [2508.13294](#).